Materials Chemistry and Physics 142 (2013) 677–681

Contents lists available at ScienceDirect

Materials Chemistry and Physics

journal homepage: www.elsevier.com/locate/matchemphys

Catalytic oxidation of *n*-hexane promoted by $Ce_{1-x}Cu_xO_2$ catalysts prepared by one-step polymeric precursor method

Vinícius D. Araújo [a,*], Maurício M. de Lima Jr. [b,c], Andrés Cantarero [b], Maria I.B. Bernardi [a], Jorge D.A. Bellido [d], Elisabete M. Assaf [e], Rosana Balzer [f], Luiz F.D. Probst [f], Humberto V. Fajardo [g]

[a] Instituto de Física, Universidade de São Paulo – USP, 13560-970 São Carlos, SP, Brazil
[b] Instituto de Ciencia de los Materiales, Universidad de Valencia, E-46071 Valencia, Spain
[c] Fundación General, Universitat de Valencia, Valencia, Spain
[d] CAP-Engenharia Química, Universidade Federal de São João Del-Rei – UFSJ, São João Del-Rei, MG, Brazil
[e] Instituto de Química, Universidade de São Paulo – USP, 13560-970 São Carlos, SP, Brazil
[f] Departamento de Química, Universidade Federal de Santa Catarina – UFSC, 88040-900 Florianópolis, SC, Brazil
[g] Departamento de Química, Universidade Federal de Ouro Preto – UFOP, 35400-000 Ouro Preto, MG, Brazil

HIGHLIGHTS

- Synthesis of CuO/CeO2 catalysts by the one-step polymeric precursor method.
- 95% *n*-hexane conversion on Ce0.97Cu0.03O2 catalyst.
- Redox properties play a key role in the catalytic performance.

ARTICLE INFO

Article history:
Received 3 January 2013
Received in revised form
23 July 2013
Accepted 16 August 2013

Keywords:
Ceramics
Chemical synthesis
Oxides
Oxidation

ABSTRACT

Ceria-supported copper catalysts ($Ce_{1-x}Cu_xO_2$, with x (mol) = 0, 0.01, 0.03, 0.05 and 0.10) were prepared in one step through the polymeric precursor method. The textural properties of the catalysts were investigated by X-ray diffraction (XRD), Rietveld refinement, N_2-physisorption (BET surface area), electron paramagnetic resonance (EPR), UV–visible diffuse reflectance and photoluminescence spectroscopies and temperature-programmed reduction (TPR). In a previous study ceria-supported copper catalysts were found to be efficient in the preferential oxidation of CO. In this study, we extended the catalytic application of $Ce_{1-x}Cu_xO_2$ systems to *n*-hexane oxidation and it was verified that the catalysts were highly efficient in the proposed reaction. The best performance (up to 95% conversion) was observed for the catalysts with low copper loads ($Ce_{0.97}Cu_{0.03}O_2$ and $Ce_{0.99}Cu_{0.01}O_2$, respectively). The physicochemical characterizations revealed that these behaviors could be attributed to the copper species present in the catalysts and the interaction between CuO and CeO_2, which vary according to the copper content.

1. Introduction

It is widely recognized that the emission of volatile organic compounds (VOCs) is a critical environmental problem and thus several techniques for the mitigation of these compounds have been investigated. Among the various approaches, catalytic oxidation is the most promising for this purpose due to advantages such as high efficiency, low operating temperature, and no secondary pollution. The design of the catalytic system is a crucial point for the success of the process. Typical catalysts for VOCs oxidation are based on noble metals (basically Pt and Pd). However, these catalysts are relatively expensive, sensitive to higher operating temperatures and sometimes their resistance to poisoning is low. Consequently, inexpensive catalytic materials like metal oxides (Cu, Co, Fe, Mn, Ce, etc.) represent attractive potential substitutes. Although these metals may be less active at low temperatures, at higher temperatures their activity can be similar

* Corresponding author. Tel.: +55 16 33739828; fax: +55 16 33739824.
E-mail addresses: dantas@ursa.ifsc.usp.br, vicodantas@yahoo.com.br (V.D. Araújo).

0254-0584/$ – see front matter © 2013 Elsevier B.V. All rights reserved.
http://dx.doi.org/10.1016/j.matchemphys.2013.08.021

to that of the noble metals [1–8]. Thus, if high-activity transition metal-based catalysts can be successfully developed for VOCs oxidation, they will be preferred. The effectiveness of cerium oxide-based catalysts in different reactions has been investigated by our research group [9–12] and have been clarified in a recent review [13]. This oxide has been commonly used as a catalyst, as well as an effective promoter for catalysts, in a wide variety of reactions since it offers redox properties and high oxygen storage capacity. In particular, it has been verified the efficiency of cu-doped ceria catalysis synthesized by a hydrothermal method in the CO preferential oxidation reaction [14–16]. Also, ceria can act as a local source or sink for oxygen involved in reactions taking place on its surface. In addition, cerium oxide is known to enhance the reducibility and the dispersion of the supported metal. In spite of these interesting characteristics, the major limitation to apply CeO_2 as a support for metallic catalysts is its low specific surface area and poor textural stability under reduction conditions [17,18].

In a previous publication [12], we described the synthesis and characterization of efficient bifunctional catalysts based on copper and cerium oxides ($Ce_{1-x}Cu_xO_2$) for the preferential oxidation of CO, achieving 100% of CO conversion. The catalysts were prepared by the one-step polymeric precursor method. This method allows an atomistic distribution of cations throughout the catalyst, improving the dispersion of cations, which is a determinant factor in catalytic reactions. In this study, we extended the catalytic application of the $Ce_{1-x}Cu_xO_2$ systems to *n*-hexane oxidation and the results are presented herein.

2. Experimental

2.1. Catalyst preparation

The CeO_2 supports were prepared by the polymeric precursor method, from the precursor salts $(NH_4)_2Ce(NO_3)_6$ – Sigma–Aldrich and $Cu(NO_3)_2{\cdot}3H_2O$ – Sigma–Aldrich [12]. Aqueous solutions of these salts were prepared, mixed and added to an aqueous solution of citric acid – Synth at 100 °C with constant stirring. The pH of the solution was adjusted to 6 with nitric acid. Subsequently, ethylene glycol ($HOCH_2CH_2OH$ – Mallinckrodt) was added to polymerize the citrate by a polyesterification reaction at 100 °C. The citric acid: metal molar ratio was 3:1, while the citric acid: ethylene glycol mass ratio was 60:40. The resulting polymer resin was then calcined at 600 °C for 2 h to produce $Ce_{1-x}Cu_xO_2$ crystalline particles, where x (mol) = 0, 0.01, 0.03, 0.05 and 0.10.

2.2. Catalyst characterization

Specific surface areas of the samples (BET–method) were estimated from the N_2-adsorption/desorption isotherms, at liquid nitrogen temperature, using a Micromeritics ASAP 2000 analyzer. The equivalent spherical diameter of the particles (d_{BET}) was calculated with the equation: $d_{BET} = 6/A_s\rho$, where A_s is the specific surface area and ρ is the density of the material in the particles.

The powders were structurally characterized with an automatic X-ray diffractometer (Rigaku, Rotaflex RU200B) with CuKα radiation (50 kV, 100 mA, λ = 1.54056 Å) equipped with a graphite monochromator. The θ–2θ configuration was used, with 2θ ranging between 20 and 90°, applying a step size of 0.02° and a step time of 5.0 s. Rietveld analysis was performed with the Rietveld refinement program GSAS [19]. A pseudo-Voigt profile function was used to account for the resolution of the system.

Electron paramagnetic resonance (EPR) spectra were recorded at 20 K on an X-band Bruker ELEXSYS E580 spectrometer. The temperature was controlled by an Oxford ITC503 cryogenic system.

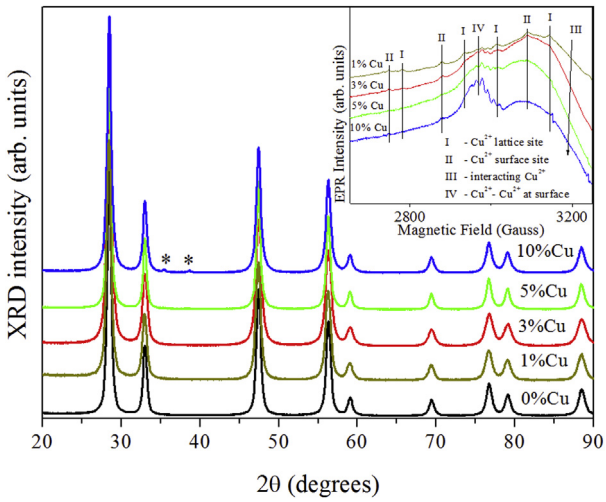

Fig. 1. XRD patterns of $Ce_{1-x}Cu_xO_2$ catalysts. Inset: EPR spectra for samples with different copper content.

The spectra were obtained at a modulation frequency of 100 kHz, modulation amplitude of 0.2 mT and microwave power of 1 mW.

UV–vis diffuse reflectance spectra were acquired with a Cary 5G spectrophotometer in the 200–800 nm range.

Photoluminescence measurements were carried out in a McPherson - 207 monochromator, with 1200 gr/mm gratings equipped with an Andor CCD. The samples were mounted in a closed-cycle Leybold cryostat, which allowed a temperature of 7 K. The 325 nm exciting wavelength of a He–Cd laser (Kimmon Koha) was used, with the nominal output power kept at 5 mW and a spot size of approximately 100 μm in diameter.

Temperature-programmed reduction (TPR) of the catalysts was performed with a multipurpose analytical system (SAMP3, Termolab Equipamentos Ltda, Brazil) and the hydrogen consumption was measured with a thermal conductivity detector (TCD). The catalyst (100 mg) was placed in the TPR reactor and reduced with a 1.96% H_2/Ar (v/v) gas mixture. The temperature was increased to 1000 °C at a heating rate of 10 °C min^{-1}. The measurement of H_2 consumption was calibrated with a standard CuO powder.

2.3. Catalytic tests

The experiments on *n*-hexane oxidation were performed under atmospheric pressure in a fixed-bed flow reactor comprised of a quartz tube with an inner diameter of 9 mm. The catalyst was placed in the middle of the reactor with thermocouples located on the top and bottom of the catalyst bed to monitor the reaction temperature. The catalyst was previously activated *in situ* under air atmosphere at 250 °C for 1 h. The gas mixture (*n*-hexane – Vetec®/air), with a flow rate of 0.12 m^3 min^{-1}, was then fed to the reactor containing 100 mg of the catalyst. The *n*-hexane/air ratio employed was 3.0 g/m^3. The reactants and the composition of the reactor effluent were analyzed on a gas chromatograph (Shimadzu GC 8A), equipped with a thermal conductivity detector (TCD), using Porapak-Q and a 5A molecular sieve column with Ar as the carrier gas. The activity of the $Ce_{1-x}Cu_xO_2$ catalysts was investigated in the temperature range of 250–450 °C. The gas chromatograph was calibrated against known concentrations of *n*-hexane and the decrease in the respective peak areas was used to measure the catalytic conversion, which was calculated as the ratio of the converted to the inlet quantity of *n*-hexane.

Table 1
Specific surface area (S_{BET}), lattice parameter (a), oxygen occupancy factor (O_{occup}), density (ρ) and equivalent spherical diameter (d_{BET}) of $Ce_{1-x}Cu_xO_2$ samples.

Sample	S_{BET} ($m^2\ g^{-1}$)	a(Å)[a]	O_{occup}	ρ ($g\ cm^{-3}$)[a]	d_{eq} (nm)
CeO_2	40.4	5.416(4)	0.97(0)	7.16	21
$Ce_{0.99}Cu_{0.01}O_2$	40.4	5.417(1)	0.95(9)	7.12	21
$Ce_{0.97}Cu_{0.03}O_2$	42.5	5.416(8)	0.96(6)	7.06	20
$Ce_{0.95}Cu_{0.05}O_2$	30.6	5.418(4)	0.95(1)	6.99	28
$Ce_{0.90}Cu_{0.10}O_2$	43.6	5.419(2)	0.96(6)	7.15	19

[a] Calculated via Rietveld refinement.

3. Results and discussion

3.1. Catalyst characterization

The catalysts in this study had been previously characterized by XRD, Rietveld refinement, N_2-physisorption – BET surface area, EPR, UV–Vis and TPR techniques and the results reported in detail in a previous publication [12]. The main results can be summarized as follows: fluorite type CeO_2 (ICSD n° 156250) was present in all samples; CuO peaks were detected only in the $Ce_{0.90}Cu_{0.10}O_2$ sample (Fig. 1); the specific surface areas of the catalysts did not vary monotonically with composition; the $Ce_{0.97}Cu_{0.03}O_2$ and $Ce_{0.90}Cu_{0.10}O_2$ samples presented the highest surface area while the $Ce_{0.95}Cu_{0.05}O_2$ sample had the lowest, as can be seen in Table 1. These results indicate that in the $Ce_{0.95}Cu_{0.05}O_2$ sample the Cu^{2+} ions were dispersed in the ceria matrix, generating oxygen vacancies, while in the $Ce_{0.97}Cu_{0.03}O_2$ and $Ce_{0.90}Cu_{0.10}O_2$ samples the CuO was probably located at the interface or on the surface of the ceria particles.

Rietveld refinement, presented in Table 1, shows the increase in the lattice parameter of the samples due to the insertion of Cu cations into the ceria matrix and the formation of oxygen vacancies in the $Ce_{0.99}Cu_{0.01}O_2$, $Ce_{0.97}Cu_{0.03}O_2$ and $Ce_{0.95}Cu_{0.05}O_2$ samples, and also the formation of a CuO phase in the $Ce_{0.90}Cu_{0.10}O_2$ sample. The $Ce_{0.99}Cu_{0.01}O_2$ and $Ce_{0.95}Cu_{0.05}O_2$ samples show the highest oxygen vacancy concentration. EPR (presented in the inset in Fig. 1) and UV–visible spectroscopies revealed that the copper is well dispersed in the $Ce_{0.99}Cu_{0.01}O_2$ and $Ce_{0.97}Cu_{0.03}O_2$ samples, located predominantly at lattice sites in the $Ce_{0.99}Cu_{0.01}O_2$ sample and at surface sites in the $Ce_{0.97}Cu_{0.03}O_2$ samples. In the $Ce_{0.95}Cu_{0.05}O_2$ and $Ce_{0.90}Cu_{0.10}O_2$ samples, the species are less dispersed than in those with lower Cu content, resulting in the formation of Cu^{2+}–Cu^{2+} dimers at the surface of the ceria. Interacting Cu^{2+} ions are present in all samples and are more predominant in the $Ce_{0.97}Cu_{0.03}O_2$ sample. TPR profiles showed reduction peaks below 400 °C for the catalysts due to the reduction of the various copper species. The different copper species are also reflected in the H_2 consumption as shown in Fig. 2. The excess H_2 consumption at low temperatures is attributed to a reduction of CeO_2 and the $Ce_{0.97}Cu_{0.03}O_2$ and $Ce_{0.90}Cu_{0.10}O_2$ samples showed greater residual H_2 consumption than the other two catalysts. The presence of Cu^{2+} cations in the CeO_2 lattice decreases the effective positive cationic charge and leads to the formation of oxygen vacancies. This decrease in the effective positive charge may give rise to a slower reduction of $Ce^{4+} \rightarrow Ce^{3+}$, explaining the lower hydrogen consumption in the case of the $Ce_{0.99}Cu_{0.01}O_2$ and $Ce_{0.95}Cu_{0.05}O_2$ samples compared with $Ce_{0.97}Cu_{0.03}O_2$ and $Ce_{0.90}Cu_{0.10}O_2$.

Fig. 3 shows the photoluminescence spectra of the samples obtained at 7 K with an excitation wavelength of 325 nm. A simple Gaussian fit of pure CeO_2 is also presented (dashed curves).

The samples could emit visible light showing a PL with a wide band that could be fitted with two Gaussians centered approximately at 637 and 729 nm. The wide band observed for the samples is attributed to sub-bands transitions within the band gap, which are closely related to surface defects and oxygen vacancies [20,21] as seen for various nanomaterials [22–24]. Interesting to note that the PL spectra for samples doped with Cu is blue-shifted compared with the pure one, and its intensity is inversely related to the O_{occup} of the samples, i.e., the lower the O_{occup} factor more intense is the PL spectra, indicating that the contribution at approximately 637 nm is attributed to the presence of oxygen vacancies. These results are in agreement with those calculated by Rietveld refinement (Table 1). In this sense, the PL spectrum for the pure sample is due to the contribution mainly from surface defects (729 nm) and oxygen vacancies (637 nm). For the samples doped with Cu, the contribution from surface defects is lower compared with pure CeO_2 due to the presence of copper species at the surface of ceria, as observed by EPR measurements.

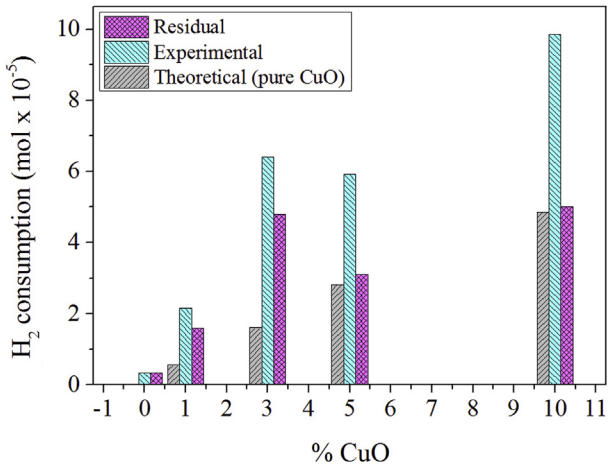

Fig. 2. H_2 consumption (theoretical, residual and experimental) on the TPR profiles obtained for the $Ce_{1-x}Cu_xO_2$ catalysts.

3.2. Catalytic tests

In order to investigate the catalytic activity of the synthesized samples, *n*-hexane oxidation reactions were carried out. The only

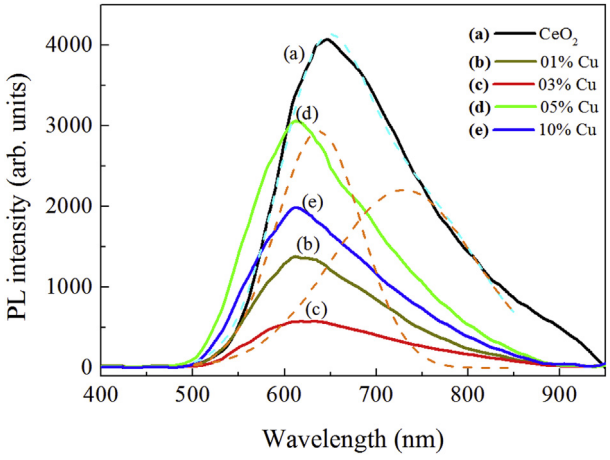

Fig. 3. Photoluminescence spectra obtained at 7 K with an excitation wavelength of 325 nm for the different catalysts. The dashed lines are a Gaussian profile fit for the CeO_2 sample.

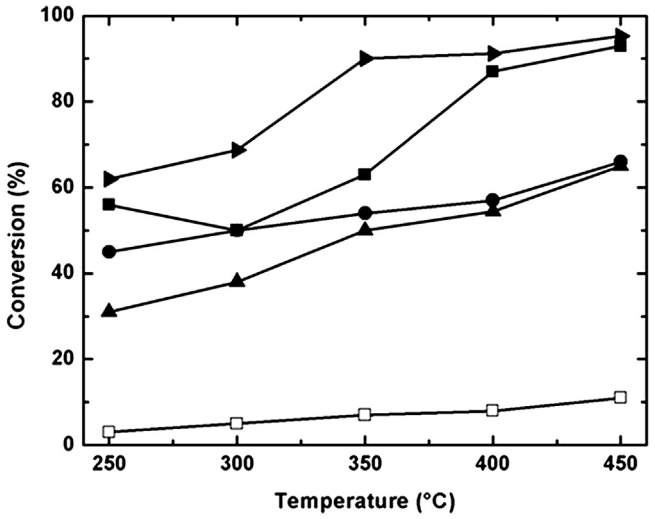

Fig. 4. Conversion as a function of reaction temperature in the *n*-hexane oxidation over different catalysts. (□) CeO_2; (■) $Ce_{0.99}Cu_{0.01}O_2$; (►) $Ce_{0.97}Cu_{0.03}O_2$; (▲) $Ce_{0.95}Cu_{0.05}O_2$; (●) $Ce_{0.90}Cu_{0.10}O_2$.

detectable reaction products in the experiments were H_2O and CO_2. Fig. 4 shows the *n*-hexane conversion for all catalysts as a function of reaction temperature.

It can be observed from the results that the catalysts were active in the studied reaction and showed a similar tendency, the *n*-hexane conversion increasing with an increase in the reaction temperature. The order of catalytic activity in the *n*-hexane reaction was as follows: $Ce_{0.97}Cu_{0.03}O_2 > Ce_{0.99}Cu_{0.01}O_2 > Ce_{0.90}Cu_{0.10}O_2 > Ce_{0.95}Cu_{0.05}O_2 > CeO_2$. The experiments show that the pure CeO_2 has no appreciable activity at the temperature range 250–450 °C. The best performance was observed for the catalysts with low copper loads ($Ce_{0.97}Cu_{0.03}O_2$ and $Ce_{0.99}Cu_{0.01}O_2$) while in the case of the $Ce_{0.95}Cu_{0.05}O_2$ catalyst, with an intermediate copper load, the *n*-hexane conversion was the lowest over the whole temperature range. These behaviors can be attributed to the copper species present in the catalysts and the interaction between CuO and CeO_2, which vary according to the copper content. The high dispersion of the copper in the catalysts with low copper contents seemed to favor the *n*-hexane conversion. Todorova et al. [25] verified that significant changes in the catalytic activity of silica-supported Mn–Co samples could be ascribed to the formation of a finely divided and uniform distribution of cobalt oxide on silica, which was reduced at lower temperatures, and enrichment of the cobalt component on the catalyst surface. The results for the EPR and UV–vis spectroscopy indicated that the copper is well dispersed in the $Ce_{0.97}Cu_{0.03}O_2$ sample and located predominantly at its surface sites. This could be the reason for the highest activity being observed for this catalyst. In another study, Todorova et al. [26] demonstrated that the lattice oxygen mobility, which is associated with the catalyst reducibility of mono-component (Co and Mn) and bi-component (Mn–Co and Mn–Ce) samples, is a very important factor responsible for the catalytic performance. According to the Rietveld refinement and PL analyses, the $Ce_{0.97}Cu_{0.03}O_2$ catalyst had the lowest formation of oxygen vacancies, indicating that, in this case, the copper species were mainly located outside the CeO_2 lattice. This is in agreement with the TPR profile, in which the second reduction peak at low temperatures, attributed to copper species with less contact with the cerium oxide support, is relatively more pronounced than in catalysts with higher copper contents ($Ce_{0.95}Cu_{0.05}O_2$ and $Ce_{0.90}Cu_{0.10}O_2$), indicating that the degree of reducibility is favored in this catalyst. The

Table 2
Comparison of published literature data with that obtained in this work.

Sample	T_{50}(°C)	T_{80}(°C)	Gas mixture	Reference
$Ce_{0.99}Cu_{0.01}O_2$	<250	~380	852 ppm in air	This study
$Ce_{0.97}Cu_{0.03}O_2$	<250	325	852 ppm in air	This study
$Ce_{0.95}Cu_{0.05}O_2$	~350	–	852 ppm in air	This study
$Ce_{0.90}Cu_{0.10}O_2$	~300	–	852 ppm in air	This study
Ce/SiO_2	330	~360	658 ppm in air	[5]
$Ce + Co/SiO_2$	271	297	658 ppm in air	[5]
Pt/Al_2O_3 (d_{Pt}-1 nm)	220	–	1500 ppm in air	[31]
Pt/Al_2O_3 (d_{Pt}-15 nm)	225	–	1500 ppm in air	[31]
SS/ZrO_2	415	525	1500 ppm in air	[32]
$SS/ZrO_2/Pt$	285	360	1500 ppm in air	[32]
$SS/ZrO_2/La_2O_3/CuCo$	315	415	1500 ppm in air	[32]

$Ce_{0.95}Cu_{0.05}O_2$ catalyst contained large amounts of type IV copper species in dimer form (due to the high proportion of copper in bulk form), which apparently did not contribute to the *n*-hexane oxidation. Although the $Ce_{0.99}Cu_{0.01}O_2$ catalyst had practically the same specific surface area as the $Ce_{0.97}Cu_{0.03}O_2$ catalyst and the copper was found well dispersed in both samples, the former showed a lower catalytic activity. This can be ascribed to the presence of type I and II copper species located predominantly at lattice sites in the $Ce_{0.99}Cu_{0.01}O_2$ sample, which is consistent with the trend toward decreased CeO_2 reduction at lower temperatures in the TPR-H_2, leading to weaker redox properties in the CeO_2 and thus a lower capacity to oxidize *n*-hexane molecules. Similar behavior was observed for the $Ce_{0.99}Cu_{0.01}O_2$ catalyst performance in the PROX reaction of CO [12]. On the other hand, in the case of the $Ce_{0.97}Cu_{0.03}O_2$ catalyst, the presence of type II (monomeric Cu^{2+} on the CeO_2 surface) and III (dipolar Cu^{2+} in 2-D nanostructures) copper species seems to be responsible for the improvement in the *n*-hexane oxidation. Moreover, the highest oxygen vacancy concentration observed for the $Ce_{0.95}Cu_{0.05}O_2$ catalyst could limit the redox properties of the Ce^{4+}/Ce^{3+} pair and thus reduce the catalyst performance. It is well known that the oxidation of hydrocarbons promoted by solid oxide catalysts can be proceeded by the Mars and van Kreveler mechanism in which the key steps are the supply of oxygen by the reducible oxide, the oxygen species introduced into the substrate molecule come from the oxide lattice, and the re-oxidation of the reduced solid by an oxygen-containing gaseous phase, which is the rate-determining step of the reaction [27,28]. According to Todorova et al. [5], the oxygen storage capacity of cerium oxide is associated with a fast Ce^{4+}/Ce^{3+} redox process, making more oxygen available for the oxidation process. The oxygen migration on the catalyst surface is important in oxidation reactions, where the oxidation–reduction cycles determine the catalytic activity. Thus, the redox properties of the catalyst play a key role in the process and are an important factor in terms of the catalytic performance. A higher surface area generally corresponds to a higher degree of dispersion of the active metallic phase and consequently higher oxidation activity due to more active sites being exposed. Another factor that may explain the low activity presented by the $Ce_{0.95}Cu_{0.05}O_2$ catalyst is its lowest specific surface area, 30.6 $m^2\ g^{-1}$ [29]. Since the specific surface area of the $Ce_{0.90}Cu_{0.10}O_2$ catalyst was only slightly larger than that of the $Ce_{0.97}Cu_{0.03}O_2$ catalyst, and the excess of H_2 consumption in the TPR experiments and the values for oxygen occupancy presented by the two catalysts were practically the same, the discrepancies observed in the catalytic activity may be due to a more prominent synergism between CuO and CeO_2 (both of which are active in the oxidation reaction) occurring in the $Ce_{0.97}Cu_{0.03}O_2$ catalyst compared with the $Ce_{0.90}Cu_{0.10}O_2$ catalyst [12]. Shan et al. [30] reported that a strong synergistic effect between copper and cerium could facilitate the reduction of CuO–CeO_2 catalysts. Thus, the catalytic

behavior of $Ce_{0.97}Cu_{0.03}O_2$ is greatly improved. According to the EPR spectra, in the $Ce_{0.90}Cu_{0.10}O_2$ catalyst the copper species are less dispersed than in those with lower copper contents, resulting in the formation of Cu^{2+}–Cu^{2+} dimers at its surface. Also, the UV–Vis diffuse reflectance spectra indicated that the $Ce_{0.97}Cu_{0.03}O_2$ catalyst presented Cu^{2+} species in an octahedral configuration, while in the $Ce_{0.90}Cu_{0.10}O_2$ catalyst the CuO showed square pyramidal or tetrahedral copper complexes. These additional factors may also be related to the differences in the catalytic behaviors observed.

Comparing the catalytic activity of the $Ce_{1-x}Cu_xO_2$ catalysts with other reported active catalysts in the *n*-hexane oxidation reaction (Table 2), it can be seen that the T_{50} (temperature for the 50% *n*-hexane conversion) is lower than 250 °C over $Ce_{0.99}Cu_{0.01}O_2$ and $Ce_{0.97}Cu_{0.03}O_2$ catalysts, and comparable to the values reported in literature for the remaining $Ce_{1-x}Cu_xO_2$ catalysts ($Ce_{0.95}Cu_{0.05}O_2$ and $Ce_{0.90}Cu_{0.10}O_2$), including T_{80}. This rough comparison of the activity with other reported catalysts indicates that the $Ce_{1-x}Cu_xO_2$ catalytic systems can be considered as a good choice for the *n*-hexane oxidation reaction.

4. Conclusions

$Ce_{1-x}Cu_xO_2$ catalysts were successfully synthesized by a one-step polymeric precursor method, characterized and tested for the oxidation of *n*-hexane. The catalysts were found to be active in the proposed reaction. The catalytic behaviors were mainly associated with the textural properties of the catalysts. The catalyst with a low copper load ($Ce_{0.97}Cu_{0.03}O_2$) presented the best performance, while for the catalyst with an intermediate copper load ($Ce_{0.95}Cu_{0.05}O_2$) the level of *n*-hexane conversion was the lowest over the whole temperature range. High dispersion of the copper on the catalyst seemed to favor the *n*-hexane conversion. EPR and UV–visible and photoluminescence spectroscopies results showed that the copper was well dispersed in $Ce_{0.97}Cu_{0.03}O_2$ catalyst and located predominantly at its surface sites. In addition, it is suggested that two copper species, monomeric Cu^{2+} on the CeO_2 surface and dipolar Cu^{2+} in 2-D nanostructures, identified in the $Ce_{0.97}Cu_{0.03}O_2$ catalyst seem to be responsible for the improved *n*-hexane conversion. The results also suggest that the redox properties of the catalysts play a key role in the process and are an important factor in terms of the catalytic performance. The $Ce_{0.95}Cu_{0.05}O_2$ catalyst presented the highest concentration of oxygen vacancies, which may limit the redox properties of the Ce^{4+}/Ce^{3+} pair and thus impair the catalytic performance. The $Ce_{0.97}Cu_{0.03}O_2$ catalyst showed the lowest formation of oxygen vacancies indicating that the copper species were mainly located outside the CeO_2 lattice. The TPR profile of this catalyst presented a second reduction peak at low temperatures, attributed to copper species with less contact with the cerium oxide support, which was more pronounced than in the case of the other catalysts, indicating that the degree of reducibility is higher for this catalyst.

Acknowledgments

The authors gratefully acknowledge the financial support of the Brazilian governmental research funding agencies FAPESP, FAPEMIG, CAPES, CNPq and the Spanish bilateral project AIB2010SE-00160. The authors are indebted to Prof. Dr. Otaciro Rangel and especially to Dr. José Fernando de Lima for the EPR measurements. The authors also would like to thank Prof. Dr. Elson Longo for the use of BET facilities.

References

[1] A.S.K. Sinha, V. Shankar, Ind. Eng. Chem. Res. 32 (1993) 1061–1065.
[2] L.F. Liotta, Appl. Catal. B Environ. 100 (2010) 403–412.
[3] A. Adamski, P. Zapała, L. Chmielarz, J.A.J. Rodriguez, G. Djéga-Mariadassou, Z. Sojka, Catal. Today 176 (2011) 318–323.
[4] S. Azalim, M. Franco, R. Brahmi, J.M. Giraudon, J.F. Lamonier, J. Hazard. Mater. 188 (2011) 422–427.
[5] S. Todorova, G. Kadinov, K. Tenchev, A. Caballero, J.P. Holgado, R. Pereñiguez, Catal. Lett. 129 (2009) 149–155.
[6] B. Grbic, N. Radic, B. Markovic, P. Stefanov, D. Stoychev, Ts. Marinova, Appl. Catal. B Environ. 64 (2006) 51–56.
[7] M. Anic, N. Radic, B. Grbic, V. Dondur, L. Damjanovic, D. Stoychev, P. Stefanov, Appl. Catal. B Environ. 107 (2011) 327–332.
[8] N. Kamiuchi, T. Mitsui, N. Yamaguchi, H. Muroyama, T. Matsui, R. Kikuchi, K. Eguchi, Catal. Today 157 (2010) 415–419.
[9] H.V. Fajardo, L.F.D. Probst, N.L.V. Carreño, I.T.S. Garcia, A. Valentini, Catal. Lett. 119 (2007) 228–236.
[10] M. Godinho, R.F. Gonçalves, E.R. Leite, C.W. Raubach, N.L.V. Carreño, L.F.D. Probst, E. Longo, H.V. Fajardo, J. Mater. Sci. 45 (2010) 593–598.
[11] A. Valentini, N.L.V. Carreño, L.F.D. Probst, A. Barison, A.G. Ferreira, E.R. Leite, E. Longo, Appl. Catal. A Gen. 310 (2006) 174–182.
[12] V.D. Araújo, J.D.A. Bellido, M.I.B. Bernardi, J.M. Assaf, E.M. Assaf, Int. J. Hydrogen Energy 37 (2012) 5498–5507.
[13] D. Zhang, X. Du, L. Shi, R. Gao, Dalton Trans. 41 (2012) 14455–14475.
[14] D. Zhang, Y. Qian, L. Shi, H. Mai, R. Gao, J. Zhang, W. Yu, W. Cao, Catal. Commun. 26 (2012) 164–168.
[15] H. Mai, D. Zhang, L. Shi, T. Yan, H. Li, Appl. Surf. Sci. 257 (2011) 7551–7559.
[16] D. Zhang, H. Mai, L. Huang, L. Shi, Appl. Surf. Sci. 256 (2010) 6795–6800.
[17] N. Laosiripojana, S. Assabumrungrat, Appl. Catal. B Environ. 66 (2006) 29–39.
[18] J.Y. Luo, M. Meng, X. Li, X.G. Li, Y.Q. Zha, T.D. Hu, Y.N. Xie, J. Zhang, J. Catal. 254 (2008) 310–324.
[19] A.C. Larson, R.B. Von Dreele, Los Alamos National Laboratory Report LAUR 86-748, 1994.
[20] J. Liqiang, Q. Yichun, W. Baiqi, L. Shudan, J. Baojiang, Y. Libin, F. Wei, F. Honggang, S. Jiazhong, Sol. Energy Mater. Sol. Cells 90 (2006) 1773–1787.
[21] C. Chai, S. Yang, Z. Liu, M. Liao, N. Chen, Chin. Sci. Bull. 48 (2003) 1198–1200.
[22] T.M. Milao, V.R. de Mendonça, V.D. Araújo, W. Avansi, C. Ribeiro, E. Longo, M.I.B. Bernardi, Sci. Adv. Mater. 4 (2012) 54–60.
[23] F. Dong, W. Zhao, Z. Wu, Nanotechnology 19 (2008) 36560.
[24] J. Liang, Z. Deng, X. Jiang, F. Li, Y. Li, Inorg. Chem. 41 (2002) 3602–3604.
[25] S. Todorova, H. Kolev, J.P. Holgado, G. Kadinov, Ch. Bonev, R. Pereñiguez, A. Caballero, Appl. Catal. B Environ. 94 (2010) 46–54.
[26] S. Todorova, A. Naydenov, H. Kolev, K. Tenchev, G. Ivanov, G. Kadinov, J. Mater. Sci. 46 (2011) 7152–7159.
[27] S. Todorova, A. Naydenov, H. Kolev, J.P. Holgado, G. Ivanov, G. Kadinov, A. Caballero, Appl. Catal. A Gen. 413–414 (2012) 43–51.
[28] J.C. Menezo, J. Riviere, J. Barbier, React. Kinet. Catal. Lett. 49 (1993) 293–298.
[29] R. Spinicci, A. Tofanari, M. Faticanti, I. Pettiti, P. Porta, Longo, J. Mol. Catal. A Chem. 176 (2001) 247–252.
[30] W. Shan, Z. Feng, Z. Li, J. Zhang, W. Shen, C. Li, J. Catal. 228 (2004) 206–217.
[31] N. Radic, B. Grbic, A. Terlecki-Baricevic, Appl. Catal. B Environ. 50 (2004) 153–159.
[32] T. Novaković, N. Radić, B. Grbić, T. Marinova, P. Stefanov, D. Stoychev, Catal. Commun. 9 (2008) 1111–1118.